Water Research 226 (2022) 119251

Contents lists available at ScienceDirect

Water Research

journal homepage: www.elsevier.com/locate/watres

Temperature response of aquatic greenhouse gas emissions differs between dominant plant types

Ralf C.H. Aben [a,b], Mandy Velthuis [a,b,c], Garabet Kazanjian [c], Thijs Frenken [b], Edwin T.H.M. Peeters [d], Dedmer B. Van de Waal [b], Sabine Hilt [c], Lisette N. de Senerpont Domis [b], Leon P.M. Lamers [a], Sarian Kosten [a,b,*]

[a] Department of Aquatic Ecology and Environmental Biology, Radboud Institute for Biological and Environmental Sciences, Radboud University, P.O. Box 9010, Nijmegen, GL 6500, the Netherlands
[b] Department of Aquatic Ecology, Netherlands Institute of Ecology (NIOO-KNAW), P.O. Box 50, Wageningen, PB 6708, the Netherlands
[c] Department of Ecosystem Research, Leibniz-Institute of Freshwater Ecology and Inland Fisheries, Müggelseedamm 301, Berlin 12587, Germany
[d] Department of Aquatic Ecology and Water Quality Management, Wageningen University, P.O. Box 47, Wageningen, PB 6708, the Netherlands

ARTICLE INFO

Keywords:
Greenhouse gas emission
Climate warming
Methane
Carbon dioxide
Ebullition
Alternative states

ABSTRACT

Greenhouse gas (GHG) emissions from small inland waters are disproportionately large. Climate warming is expected to favor dominance of algae and free-floating plants at the expense of submerged plants. Through different routes these functional plant types may have far-reaching impacts on freshwater GHG emissions in future warmer waters, which are yet unknown. We conducted a 1,000 L mesocosm experiment testing the effects of plant type and warming on GHG emissions from temperate inland waters dominated by either algae, free-floating or submerged plants in controls and warmed (+4 °C) treatments for one year each. Our results show that the effect of experimental warming on GHG fluxes differs between dominance of different functional plant types, mainly by modulating methane ebullition, an often-dominant GHG emission pathway. Specifically, we demonstrate that the response to experimental warming was strongest for free-floating and lowest for submerged plant-dominated systems. Importantly, our results suggest that anticipated shifts in plant type from submerged plants to a dominance of algae or free-floating plants with warming may increase total GHG emissions from shallow waters. This, together with a warming-induced emission response, represents a so far overlooked positive climate feedback. Management strategies aimed at favouring submerged plant dominance may thus substantially mitigate GHG emissions.

1. Introduction

Shallow, freshwater ecosystems typically represent a specific ecological state, characterized by the dominance of different functional plant types: submerged plants, phytoplankton, or free-floating plants (Scheffer and Carpenter, 2003; Scheffer and van Nes, 2007). Shifts between these ecological states can occur rather sudden, for instance due to storms or water level changes (see Scheffer (1998)). These so-called alternative states affect primary production, biogeochemical processes, and important ecosystem services (Carpenter and Lodge, 1986; de Tezanos Pinto and O'Farrell, 2014; Hilt et al., 2017; Janssen et al., 2021). While blooms of all primary producers can lead to anoxia under eutrophic conditions (e.g. Istvánovics, 2009), in mesotrophic conditions dominance by free-floating plants such as *Lemna*, for instance, typically leads to much lower oxygen concentrations in the water and sediment as compared to submerged plant and algae dominated states (Netten et al., 2010). This is mainly due to decreased phytoplankton photosynthesis below the shading plant canopy, decreased diffusion of oxygen through the plant mats, and decaying plant matter resulting in high sediment oxygen demand (de Tezanos Pinto and O'Farrell, 2014). These low oxygen conditions potentially promote methane (CH_4) emission. Shifts in dominance of different types of plants may therefore have far-reaching implications for freshwater greenhouse gas (GHG) emissions (Hilt et al., 2017; Li et al., 2021). Comparisons of GHG (carbon dioxide, CO_2; CH_4; and nitrous oxide, N_2O) emissions between distinct alternative states have so far been based on a limited number of field observations,

* Corresponding author at: Department of Aquatic Ecology and Environmental Biology, Radboud Institute for Biological and Environmental Sciences, Radboud University, P.O. Box 9010, Nijmegen, GL 6500, the Netherlands.
E-mail address: Sarian.Kosten@ru.nl (S. Kosten).

https://doi.org/10.1016/j.watres.2022.119251
Received 18 March 2022; Received in revised form 11 October 2022; Accepted 13 October 2022
Available online 17 October 2022

and have been complicated by a range of confounding factors, such as a lack of standardized methods, and the omission of certain GHGs as well as their relevant emission pathways—such as CH_4 ebullition (bubble flux of CH_4 from sediments) (Hilt et al., 2017; Li et al., 2021). Hence, it remains unclear how shifts in plant dominance will affect GHG emissions.

Based on the increase of individual metabolic rates it is expected that higher temperatures will disproportionally increase ecosystem respiration relative to gross primary production (Allen et al., 2005; Yvon-Durocher et al., 2010), which may lead to a reduced net CO_2 uptake. While some studies confirm this effect of warming (Yvon-Durocher et al., 2017), others do not find such an effect (Davidson et al., 2015), or even find a lower net CO_2 efflux with warming (Davidson et al., 2015). These contrasting results may be due to differences in the availability of growth-limiting resources (e.g. nitrogen and phosphorus), food web structure, as well as indirect effects of temperature. The latter includes effects of temperature on the abundance, growth strategies, and key traits of the plants and microorganisms present, which may override the effects of temperature on the metabolic rates at the subcellular and individual level (Davidson et al., 2015; Dossena et al., 2012; Hood et al., 2018; Kraemer et al., 2017).

Similarly, effects of temperature on CH_4 emission are ambiguous. Although CH_4 production by methanogenic Archaea (mainly in sediments) tends to be temperature dependent when sufficient substrate is available (Fuchs et al., 2016; Marotta et al., 2014), not all CH_4 reaches the atmosphere as part of it is subject to microbial oxidation of CH_4 (mainly in the sediment-water interface and water column) (Bastviken et al., 2009), a process which is also temperature dependent (Fuchs et al., 2016; Lofton et al., 2014; Shelley et al., 2015). Differential temperature effects on CH_4 production and CH_4 oxidation (Fuchs et al., 2016; Lofton et al., 2014; Shelley et al., 2015) as well as warming-induced shifts in the microbial community (Zhu et al., 2020), may explain the differential effects of warming on diffusive CH_4 emissions reported in the literature, varying from positive effects to the absence of effects (Aben et al., 2017; Davidson et al., 2015; Yvon-Durocher et al., 2014; Zhu et al., 2020). The effect of warming on CH_4 ebullition, however, seems unambiguous, as reports so far indicate a strong increase with warming—provided that substrates for CH_4 production are not limiting (Aben et al., 2017; Davidson et al., 2018; Del-Sontro et al., 2016). CH_4 ebullition largely bypasses microbial CH_4 oxidation and is often found to be the dominant GHG emission pathway in inland waters (Bastviken et al., 2009). Despite this, ebullition is often not measured, or only measured at short time intervals (minutes to hours), which likely results in an underestimation of this strongly episodic flux (Hilt et al., 2017; Saunois et al., 2016; Wik et al., 2016). To date, however, most ebullition measurements have been conducted at unvegetated sites (e.g. Aben et al. (2017)). Furthermore, ebullition data recorded over a considerable temperature range are rare for systems dominated by submerged plants (but see Davidson et al. (2018)) and even more so for systems dominated by free-floating plants, possibly due to methodological difficulties (see Methods). Yet, these functional plant types can strongly modify CH_4 production, consumption and transportation (see Bodmer et al. (2021) for an overview of the different processes) thereby likely leading to a differential temperature effect on CH_4 ebullition under contrasting ecosystem states. However, although climate warming can increase the chances of shifts from dominance by submerged plants to dominance by free-floating plants or algae (Mooij et al., 2007; Netten et al., 2011; Peeters et al., 2013), not much is known about the consequences of these shifts for GHG emissions in general (Hilt et al., 2017) and ebullition in particular. The question therefore remains how dominance of different functional plant types in shallow lakes and ponds will affect GHG emissions and the impact of climate warming on these emissions. To answer this fundamental question, we used indoor ~1000 liter experimental ponds containing natural lake sediments and overlaying water, and experimentally tested in three consecutive years how warming (+4 °C; $n = 4$) affected year-round GHG emissions in the temperate climate zone under dominance of different functional plant types (dominance by submerged plants, *Myriophyllum spicatum;* free-floating plants, *Lemna minor / Spirodela polyrhiza;* or algae). We measured emissions of all important GHGs (i.e. CO_2, CH_4, and N_2O) and the contributions of their relevant emission pathways.

2. Materials and methods

2.1. Experimental setup

The experiment was conducted in eight cylindrical, stainless steel, indoor mesocosms called limnotrons, with a volume of 988 L, a depth of 1.34 m and a diameter of 0.97 m (area 0.74 m^2), situated at the Netherlands Institute of Ecology [see Verschoor et al. (2003) for details]. For this study, limnotrons were set up to mimic shallow, temperate latitude ponds and lakes with moderate nutrient concentrations: systems where alternative states are possible (Scheffer and van Nes, 2007). Starting in 2014 three states with dominance of different types of plants were studied consecutively, each for a full year: an algae, submerged plant, and free-floating plant-dominated state. Temperature treatments consisted of a control ($n = 4$), with seasonally-varying water temperatures typical for Dutch lakes (Fig. 2), and a warm (+ 4 °C) treatment, consistent with predicted warming by the end of the 21st century in North and Central Europe under intermediate anthropogenic GHG emissions [scenario RCP6.0 (IPCC, 2013)]. Both temperature treatments included a five-day midsummer heat wave (+ 4 °C), as heat waves are expected to occur more often in the future (IPCC, 2013). As we do not have a control for the heat wave, we refrain from speculating about its effects. The light/dark cycle followed Dutch seasonality, with 17 h of daylight in midsummer, and 8 h of daylight in midwinter. The limnotrons were emptied and cleaned for each state: soft, muddy sediment was collected from a nearby mesotrophic pond (51°59′16.0″N, 5°40′06.1″E), sieved over a 5 mm mesh and homogenized by thorough manual mixing before adding it to the limnotrons. Approximately 75 L of sediment was added to each limnotron ± two weeks before the start of the experiment of each plant type. Sediment organic C and C:N ratios (Table 1) were similar to those of shallow lakes and ponds with a similar trophic state (Gilbert et al., 2021; Marotta et al., 2014). To maintain sediment characteristics as similar as possible for the different states while also mimicking approximate sediment conditions that correspond to the different functional plant types dominating the system, we used sediment from the above-mentioned pond for all three states. For the submerged plant state we mixed sediment collected the year before with fresh sediment (1 to 2 parts, v/v) to ensure the presence of fresh organic matter. For the free-floating plants state freshly collected sediment from the pond was mixed with sediment from the previous state (1 to 14 parts, v/v). Duckweed dominance is stabilized by the presence of propagules in the sediment (Boedeltje et al., 2005). Hence, we subsequently spiked (1 to 28 parts, v/v) the systems with sediment from a nearby duckweed-dominated ditch (51°59′43.3″N, 5°38′38.7″E). After the introduction of the sediment, the limnotrons were filled to the top with tap water. Water was circulated manually between all limnotrons for 2 days to ensure homogeneous starting conditions. An aquarium pump (EHEIM compact 300; EHEIM GmbH & Co. KG, Deizisau, Germany) and two compact axial fans (AC axial compact fan 4850 Z; EBM-papst St. Georgen GmbH & Co. KG, Georgen, Germany) with an air flow of 100 $m^3\ h^{-1}$ were installed above each limnotron to promote a gas exchange velocity typical of small lakes and ponds (see Supplementary Methods for details). Lastly, limnotrons were spiked with nutrients and the different types of plants were introduced at densities typical for the respective state (see below for details). Limnotrons were left to establish for ca. 2 weeks prior to experimental warming at temperatures of ca. 5 (control) and 8 (warmed)°C. Throughout the experiment, limnotrons were gently refilled with demineralized water once or twice per week to compensate for evaporative losses.

Table 1
Annual means ± standard deviations of ebullition as percentage of total CH_4 flux, oxygen, oxygen saturation, dissolved CH_4, major nutrients, sediment organic C:N, sediment organic C, sedimentation rates, added plant biomass and harvested biomass for each of the three plant-dominated states and their treatments. $n = 4$ on all instances. Each n represents the annual average value of the respective variable per limnotron. Annual averages of time series concentration data (O_2, dissolved CH_4 and nutrients) were calculated by dividing the area under the curve—calculated using numerical integration with Simpson's rule (function *sintegral* of package 'Bolstad2' (Curran, 2013)—by the number of sampling days of each timeseries.

State	Sediment Org-C:N (atomic)[c]	Sediment Org-C (%)[c]	Ebullition as % of total CH_4 flux(control)	Ebullition as % of total CH_4 flux (+4°C warmed)	Oxygen (mg L^{-1})[a](control)	Oxygen (mg L^{-1})[a](+4°C warmed)
Submerged plant	13.7 ± 1.7	4.0 ± 1.6	57.9 ± 5.9	72.6 ± 6.0	9.04 ± 0.75	8.88 ± 1.07
Free-floating plant	12.8 ± 0.4	3.5 ± 0.6	80.3 ± 12.1	93.1 ± 5.4	1.51 ± 0.61	1.53 ± 0.17
Algae	12.8 ± 0.4	1.4 ± 0.1	90.2 ± 2.8	94.9 ± 0.8	8.15 ± 0.49	8.42 ± 1.30
State	**Oxygen saturation (%)** (control)	**Oxygen saturation (%)** (+4°C warmed)	**CH_4 (µg L^{-1})**[b] (control)	**CH_4 (µg L^{-1})**[b] (+4°C warmed)	**NH_4-N (µg L^{-1})** (control)	**NH_4-N (µg L^{-1})** (+4°C warmed)
Submerged plant	79.8 ± 7.4	86.4 ± 9.6	16 ± 1	17 ± 6	57 ± 17	53 ± 14
Free-floating plant	14.5 ± 6.0	17.3 ± 2.0	184 ± 117	65 ± 18	464 ± 55	597 ± 290
Algae	74.3 ± 4.6	83.8 ± 13.4	20 ± 8	15 ± 2	446 ± 106	376 ± 227
State	**NO_3-N (µg L^{-1})** (control)	**NO_3-N (µg L^{-1})** (+4°C warmed)	**PO_4-P (µg L^{-1})** (control)	**PO_4-P (µg L^{-1})** (+4°C warmed)	**Sedimentation (mg C m^{-2} d^{-1})**[d] (control)	**Sedimentation (mg C m^{-2} d^{-1})**[d] (+4°C warmed)
Submerged plant	78 ± 12	69 ± 9	25.1 ± 0.4	25.0 ± 0.3	382 ± 82	598 ± 202
Free-floating plant	442 ± 473	471 ± 53	127.7 ± 44.2	118.8 ± 22.6	611 ± 146	720 ± 157
Algae	262 ± 61	327 ± 120	5.7 ± 0.4	6.3 ± 0.6	156 ± 32	178 ± 78
State	**Added biomass (g C m^{-2})**[e,f]	**Final biomass (g C m^{-2})**[g] (control)		**Final biomass (g C m^{-2})**[g] (+4°C warmed)		
Submerged plant	9.8 ± 3.0	12.8 ± 5.1		24.7 ± 3.2		
Free-floating plant	35.0 ± 0.1	60.6 ± 5.6		51.8 ± 23.1		
Algae	2.2 ± 0.4	3.5 ± 2.9		3.8 ± 5.1		

[a] Values represent averages of water column depth profile measurements taken throughout the year around noon.
[b] Concentrations correspond to the upper 10 cm of the water column measured multiple times per year.
[c] Sediment was sampled at the start of each experiment. Since starting conditions were similar for treatments, we did not differentiate between control and warm treatment.
[d] Assessed during the first 6 months of the experiments.
[e] Since starting conditions were similar for treatments, we did not differentiate between control and warm treatment.
[f] C of added submerged plant biomass was calculated by multiplying the estimated dry weight of added submerged plant matter by their carbon content after harvest (Velthuis et al., 2018). Total C of added free-floating plant biomass was determined by multiplying the measured wet weight (WW) of added plant biomass by the dry weight:wet weight (DW:WW) ratio determined after harvest. Subsequently, the calculated DW was multiplied by the measured C fraction of the plants (determined after harvest). C in added algae biomass was determined by multiplying the measured sestonic C content of a filtered water sample (Velthuis et al., 2017) at the start of the experiment by the volume of the water column. These numbers were divided by the limnotron surface area to obtain values in g C m^{-2}.
[g] Harvested at the end of the experiment.

2.2. Plant characteristics

For the algae-dominated state, limnotrons were inoculated with a phytoplankton community from the same mesotrophic pond where the sediment was collected, and an additional (<15%) inoculum from a nearby eutrophic pond (51°59′16.3″ N 5°40′06.0″ E) on 15 February 2014. This resulted in an initial biomass of 2.2 ± 0.4 g C m^{-2} (Table 1), typical for temperate mesotrophic freshwater bodies in spring (e.g. Nixdorf and Arndt (1993)). For the submerged plant-dominated state, the species *Myriophyllum spicatum* (Eurasian watermilfoil) was used, as this plant is a common native or naturalized species in most temperate climate regions (GRIN database [https://www.ars-grin.gov/npgs; verified 23 January 2018]). Plants with a median length of about 80 cm including roots were collected from the pond the sediment originated from in March 2016 and carefully washed to remove macroinvertebrates and their eggs. We introduced five plants to each mesocosm by tying a pebble just above their roots to sink them to the sediment. Due to limited initial growth, four and six additional plants were added to each limnotron in the same way at seven and sixteen weeks after the start of the experiment, respectively. This resulted in a plant density of 20 per m^2 and a total initial biomass of 9.8 ± 3.0 g C m^{-2} (Table 1; 11–31 g dry weight m^{-2}, approximately 140 g fresh weight (FW) per limnotron, PVI < 1%), which represents a typical spring situation in temperate *M. spicatum* stands (e.g. Tóth and Herodek (2011)). Biomass of added submerged macrophytes was estimated using photographs of the plants added to each limnotron and converting the plant surface area on the photo to a dry weight biomass as explained in Fig. S1. For the free-floating plant-dominated state, a community of duckweed species (mainly *Lemna minor* & *Spirodela polyrhiza*) was collected on 19 April 2016 from an agricultural ditch (in Ysselsteyn, the Netherlands) and introduced to the limnotrons. The mentioned duckweed species are native and common free-floating plants in most temperate climate regions (Hussner (2012) & GRIN database [https://www.ars-grin.gov/npgs; verified 23 January 2018]). Directly after collecting, the duckweed was carefully sieved (mesh size 0.85 mm) and washed to remove litter as well as macroinvertebrates and their eggs. We then introduced 500 g FW of duckweed to each limnotron, which resulted in 100% surface cover which is typical for temperate waterbodies dominated by duckweed (e.g. Kazanjian et al. (2018a)). Throughout the year, the community was dominated by *Lemna minor* and *Spirodela polyrhiza*. The

cold water at the start of the experiment combined with the thin plant mat likely delayed the onset of low-oxygen conditions and related nutrient release (de Tezanos Pinto and O'Farrell, 2014), thereby hampering duckweed growth. To overcome this growth constraint and to hasten the development of hypoxic conditions, we added extra biomass (600 g FW) to each limnotron on day of year (DOY) 29. During the second half of the experiment, we experienced a large die-off of free-floating plants due to infection by *Cataclysta lemnata* larvae (also known to occur in systems outdoors [e.g. Arts et al. (2001)]). To compensate for this we re-introduced biomass (400 g FW) to each limnotron on DOY 211. Total C added to each limnotron via biomass introduction was 35.0 ± 0.1 g C m^{-2} (Table 1). Throughout the experiment, duckweed covered on average 90 (63–100)% of the surface in the control and 94 (50–100)% in the warm treatment [mean (min–max)].

2.3. Temperature, light & nutrients

Water temperature was directly thermostat-regulated (± 0.2 °C), using a custom made climate control system running on SpecView software (SpecView 32/859, SpecView Ltd.), and containing active heating and cooling elements, and PT100 temperature sensors at depths of 0.5 and 1.0 m. Water temperature was logged at intervals of 1 min by the climate control system and was additionally checked throughout the experiment during regular depth profile measurements of oxygen, light, temperature, and pH. Oxygen, temperature, and pH were measured using a multi-parameter meter (HQ40d, Hach, Loveland, CO, USA) equipped with a luminescent/optical dissolved oxygen (LDO) probe (IntelliCAL LDO101) and a pH probe (PHC10105). Light intensity was measured using a UW Quantum light sensor (LI-COR Environmental GmbH, Bad Homburg, Germany). For each limnotron, light was provided by two HPS/MS lamps (CDM-TP Elite MW 315–400 W, AGRILIGHT B.V.), resulting in a constant incident light intensity of 160 ± 40 (PAR; mean ± s.d.) µmol photons m^{-2} s^{-1}. Limnotrons were spiked with nutrients at the start of each experiment, to reach start concentrations of 4.2 ± 0.8, 0.2 ± 0.1, and 4.3 ± 1.0 mg L^{-1} of NO_3^-, PO_4^{3-}, and Si, respectively. These concentrations both fall within the overlapping ranges of a mesotrophic and eutrophic state according to the quantitative lake classification tables of Vollenweider and Kerekes (1980). We chose these concentrations as they allow for phytoplankton, submerged macrophyte as well as floating plant dominance. Minor nutrient losses through sampling were recorded and compensated for by weekly nutrient additions. To determine concentrations of dissolved nutrients in the surface water, 10 mL of water sample was filtered over a prewashed (100 mL distilled water) glass microfiber filter (Whatman GF/F, Maidstone, UK) and stored at −20 °C until analysis. Prior to analysis, samples were slowly thawed at 5 °C. Concentrations of ammonium (NH_4^+), nitrate (NO_3^-), and phosphate (PO_4^{3-}) were measured on a QuAAtro39 AutoAnalyzer (SEAL Analytical Ltd., Southampton, UK). Sediment pore water was sampled anaerobically using 60 mL vacuum syringes connected to Rhizon pore water samplers (Rhizon MOM, 0.15 µm pore size; Rhizosphere Research Products, Wageningen, The Netherlands) installed in the upper 10 cm of the sediment. The first 10 mL was discarded to enable anaerobic sampling. Samples were stored at −20 °C until further analysis. Pore water concentrations of PO_4^{3-}, NO_3^- and NH_4^+ were measured colorimetrically with an Auto Analyzer 3 system (Bran+Luebbe, Norderstedt, Germany), using ammonium molybdate (Henriksen, 1965), hydrazine sulfate (Kamphake et al., 1967) and salicylate (Grasshoff and Johannsen, 1972), respectively. Total inorganic nitrogen (N) was determined by summing the ammonium (NH_4^+) and nitrate (NO_3^-) concentrations. Dried plant biomass was ground to a fine powder on a microfine grinder (MF 10 basic; IKAwerke, Staufen, Germany). C and N content was analyzed on a FLASH 2000 NC elemental analyzer (Brechbuehler Incorporated, Interscience B.V., Breda, The Netherlands). Phosphorus content was determined by combustion of plant biomass in a Pyrex glass tube at 550 °C for 30 min (Murphy and Riley, 1962). Subsequently, 5 mL of persulfate (2.5%) was added and samples were autoclaved for 30 min at 121 °C. Digested P (as orthophosphate) was measured colorimetrically on a QuAAtro39 Auto--Analyzer (SEAL Analytical Ltd., Southampton, UK).

2.4. Ebullitive fluxes

Throughout the experiment, CH_4 release via ebullition was determined by continuous collection of gas bubbles from the sediment, using custom made bubble traps. Bubble traps consist of an inverted funnel (ID 15.2 cm) connected to a water-filled glass container via an 80 cm long tube (ID 10 mm). Each limnotron contained two bubble traps, with funnels being approximately 50 cm under the water surface. Gas filled glass containers were collected (and immediately replaced by new ones) a total of 10, 13, and 13 times during the submerged plant, free-floating plant, and algae dominated states, respectively, always before being completely filled with gas. The deployment time of glass containers before being replaced depended on the ebullition rate and ranged from 11 to 89 (median: 25), 7 to 64 (median: 18), and 8 to 65 (median: 21) days in the submerged plant, free-floating plant, and algae dominated states, respectively. After collection, the volume of gas was determined by subtracting the weight of each bottle from the pre-determined full filled-weight (i.e., bottle completely filled with water). CH_4 concentrations in the gas were measured on an HP 5890 gas chromatograph equipped with a Porapak Q column (80/100 mesh) and a flame ionization detector (Hewlett Packard, Palo Alto, CA, USA). The amount of gaseous CH_4 in each bottle was determined by multiplying the CH_4 concentration (C_{gas}) by the volume of gas (V_{gas}). The CH_4 in the bottles was assumed to be in equilibrium with the water phase. Hence, the amount of CH_4 dissolved in the water (C_{water} * V_{water}) was calculated using Henry's law and its solubility constant for CH_4, taking the respective water temperature into account (Sander, 2015). The total amount of CH_4 in each bottle was calculated by summing the aqueous and gaseous content and divided by funnel surface (A) and time (Δt) to calculate CH_4 ebullition per square meter (Eq. (1)):

$$n\_CH_4 = \frac{(C_{gas} * V_{gas}) + (C_{water} * V_{water})}{\Delta t * A} \quad (1)$$

The CH_4 content of collected ebullitive gas was on average 45 (0–91)%, 76 (0–99)%, and 57 (0–95)% (min–max) for the submerged plant, free-floating plant, and algae dominated states, respectively. Gas volume in glass containers was checked on several occasions before and after diffusive flux measurements to assess whether measurements triggered bubble release. We observed no effect. Prior to the harvest of submerged plants, random plant stems were broken and evolving gas bubbles were captured by enclosing the stem with inverted, water-filled 12 mL gas-tight vials (Exetainer®, Labco, Lampeter, UK). Subsequently, CH_4 concentrations of captured gas were determined as described above. Estimating CH_4 ebullition in free-floating plant dominated systems is not straightforward, as part of the evolved bubbles are trapped under dense free-floating plant mats. Based on plant cover and the empirical relationship reported in Kosten et al. (2016) we assumed that in our systems 20% of measured ebullition was trapped. We therefore reduced the ebullitive flux measured below the free-floating plants with 20% to get an estimate of the ebullitive emission to the atmosphere. CH_4 from trapped bubbles may partially dissolve and can be consumed by microbes in the aerobic rhizosphere of the free-floating plants (Kosten et al., 2016).

2.5. Diffusive greenhouse gas fluxes

Diffusive fluxes of CH_4 and CO_2 were measured using an acrylic, cylindrical, transparent chamber (ID 29.2 cm) connected in a closed loop to a greenhouse gas analyser (GGA). During the first six months of the algae-dominated state, CH_4 concentrations were measured using Off-Axis Integrated-Cavity Output Spectroscopy GGA (model GGA-24r-EP, Los Gatos Research), while CO_2 concentrations were determined

from pH, temperature, and dissolved inorganic carbon measurements (see following paragraph). All measurements of N_2O, CH_4 and CO_2 thereafter were conducted using a wavelength-scanned Cavity Ring-Down Spectroscopy GGA (model G2508, Picarro). Both devices measured at 1 Hz intervals and yielded similar results in a post-experiment comparative test, ensuring no analyser-related bias. Measurements of 3–5 min were performed in triplicate and were repeated when influenced by ebullition (evidenced as an abrupt concentration increase). In between measurements, the chamber was ventilated with ambient air. Diffusive fluxes were typically measured every 2–4 weeks (dominance by submerged and free-floating plants) and every 2 weeks (dominance by algae) during the pre-heat wave period, and every 4–5 weeks during the post-heat wave period. In all cases, additional measurements were performed in the week before, during, and after the heat wave. The slope of the relationship between gas concentration and time was used to calculate fluxes (DelSontro et al., 2016) (Eq. (2)):

$$F = \frac{V}{A}*\text{slope}*\frac{P*F1*F2}{R*T} \quad (2)$$

where F is the gas flux (g m^{-2} d^{-1}), V is chamber headspace volume (m^3; measured during the measurement) and A is chamber surface area (m^2), slope is the slope of the relationship between the GHG concentration and the time (ppm $second^{-1}$); P is atmospheric pressure (Pa); $F1$ is the molar mass of the respective GHGs: CO_2 (44.01), N_2O (44.01) or CH_4 (16.04) (g mol^{-1}); $F2$ is the conversion factor of seconds to days; R is the ideal gas constant 8.3145 (m^3 Pa K^{-1} mol^{-1}); T is the water temperature (K).

In the free-floating plant-dominated state, deployment of the floating chamber during warm periods with high ebullition led to an initial peak in CH_4 concentration (even in replicate measurements) followed by a strong, linear increase over the following minutes. Only the latter was used to calculate the diffusive flux. Both the initial peak as well as the large magnitude of the diffusive flux are likely caused by the release of CH_4 from trapped bubbles under the plant mats (as described above). Although part of this gaseous CH_4 may have diffused to the atmosphere also without the disturbance of the floating chamber deployment we subtracted the fraction of ebullition estimated to be retained under the plant mats (described above) from the measured diffusive flux. We argue that we hereby obtained a conservative estimate of the diffusive CH_4 flux, as under natural conditions, wind and animals (e.g. birds & fish) can displace floating plant mats, which would further enhance CH_4 emissions to the atmosphere.

Diffusive fluxes were always measured at the end of the day as well as at the end of the night period to capture expected minimum and maximum fluxes of CO_2, respectively. Mean diel fluxes of CH_4 and CO_2 were calculated as a weighted average of the light and dark period fluxes, based on day- and nighttime length. Limnotrons were always measured in random order to avoid potential bias by time- or order-related effects. A leakage test was performed on each measurement day to ensure no leakage was present in the closed-loop system. To this end, the chamber base was sealed to a flat surface using Terostat IX (Teroson). The opening at the top of the chamber was then closed with a cap containing a septum through which methane was injected. A CH_4 concentration of approximately 15 ppm was then used to check for leakages over a 20–30 min period. No leakages were detected. Throughout the experiment, we observed no emission of N_2O except for day 196 of the experiment, where N_2O emission was observed in a control mesocosm of the algae-dominated state (4.8 mg N_2O m^{-2} d^{-1}). Hence, N_2O emission was of trivial importance for the overall GHG emissions and therefore not included in our analyses.

2.6. Calculated CO_2 water-atmosphere fluxes

Though the majority of diffusive CO_2 fluxes were measured using a GGA (as discussed above), this was not possible during the first six months of the experiment with algae as the dominant primary producer, due to a malfunctioning CO_2 sensor in the Los Gatos GGA. During this period, we determined CO_2 fluxes as follows (Eq. (3)):

$$F = k\left(C_{sur} - C_{eq}\right) \quad (3)$$

where F is the flux (mg CO_2 m^{-2} d^{-1}), k is the piston velocity (m d^{-1}), and C_{sur} and C_{eq} are surface water and air-equilibrium CO_2 concentrations (mg CO_2 m^{-3}) Cole et al., 2010), respectively. Piston velocity (as kO_2) was empirically determined at temperatures of 8.5, 16.5 and 24.5 °C in an additional limnotron that did not contain sediment, using deoxygenated water (after Tribe et al. (1995). The data of these experiments can be found in Fig. S2 Standardizing these k measurements (by respective Schmidt numbers and an exponent n of −0.67 for low-wind systems (Cole et al., 2010; Wanninkhof, 2014)) resulted in a k_{600} of 0.43 ± 0.03 m d^{-1} (mean ± s.d.; Fig. S3), which is typical for small lakes and ponds (Holgerson and Raymond, 2016). C_{sur} was calculated from measurements of dissolved inorganic carbon (DIC), pH, temperature, and dissociation constants of carbonic acid in pure water (Millero et al., 2006) according to the equations in Table 4.2 of Stumm and Morgan, 1996. C_{eq} was calculated using Henry's law and its solubility constant for CO_2 (after Sander (2015)), taking the respective water temperatures into account and assuming an atmospheric CO_2 fraction of 400 ppm. At high pH the chemical reaction of CO_2 with OH^- in the water-atmosphere boundary layer can significantly increase the mass transfer of CO_2 from the air to the water, a process referred to as 'chemical enhancement of CO_2 exchange' (Bade and Cole, 2006). Chemically enhanced diffusion was taken into account by, in case of CO_2 uptake, multiplying k by a chemical enhancement factor (β) which depends on pH, temperature, and k itself, following Eqs. (4)–((6) in Bade and Cole (2006). Also, for each calculation of F, k was adjusted for water temperature at time of DIC sampling (Cole et al., 2010; Wanninkhof, 2014). Minimum and maximum CO_2 fluxes were calculated using pH measurements at the end of the light and end of the dark period. The mean diel flux of CO_2 was calculated as a weighted average of the light and dark period fluxes, based on day- and nighttime length. The reliability of this method was verified later in the experiment, when CO_2 fluxes measured by the Picarro GGA were compared with fluxes calculated from 10 cm deep DIC, temperature, and pH measurements, taken directly after the Picarro GGA measurements. There was a strong relationship between data of the two methods ($R^2 = 0.96$) (Fig. S4). The regression of this relationship was used to adjust the calculated CO_2 fluxes for standardization.

2.7. Dissolved inorganic carbon

Samples for DIC were carefully collected (to prevent gas exchange) once a week and stored in 3 mL non-evacuated gas-tight vials (Exetainer®, Labco, Lampeter, UK) at 4 °C. DIC was measured within 24 h after sampling by injecting a 0.2 mL sample in a closed glass chamber containing 0.2 M H_3PO_4 solution, converting the DIC into CO_2. Subsequently, a continuous flow of N_2 gas transported the CO_2 to an AO2020 Continuous Gas Analyser (ABB, Zürich, Switzerland). A calibration curve was made by injecting different volumes (0.1–1.0 mL) of 1.25 mM HCO_3^- solution in order to convert raw instrument output to DIC mass.

2.8. Sedimentation

Each month, sedimentation was determined by installing custom-made tube-shaped sedimentation traps (9 cm diameter, 19 cm height, 1.1 L volume) at 1 m depth below the water surface in the center of the limnotron for 3 days. Contents of the sedimentation trap (i.e., sedimented material and sestonic particulate organic carbon (POC) in the water inside the trap) were subsequently filtered using pre-washed GF/F filters (Whatman, Maidstone, UK), dried overnight at 60 °C, and stored dry and dark for elemental analysis. During collection of the sedimentation traps, surface water was sampled using a 1 m long tube sampler in the center of the limnotron and analysed as described above to correct

for sestonic POC (<220 μm). Sedimentation rates were calculated as the amount of sedimented POC (corrected for sestonic POC present inside the traps) divided by the deployment time of the sedimentation traps. Finally, the amount of sedimented organic carbon was calculated as the area under the curve of these sedimentation rates.

2.9. Sediment analyses

Homogenized sediment samples were oven dried for 2 days at 70 °C. Subsequently, a Mixer Mill MM 400 (Retsch GmbH) was used to grind the dried sediment samples. 25 mg of fine grind sediment was weighed in silver capsules and exposed to repeated additions of 10 μL of 25% HCl to remove carbonates (Nieuwenhuize et al., 1994). Samples were then analysed for organic carbon and nitrogen content using an NA 1500 elemental analyser (Carlo Erba).

2.10. Plant abundance

Submerged plant abundance was measured by weekly PVI (Percent Volume Infested) estimates, where plant height was measured with a ruler and cover% was visually estimated. PVI of *Myriophyllum spicatum* was then calculated according to Canfield Jr et al. (1984) (Eq. (4)):

$$\mathrm{PVI} = \frac{\text{plant cover*plant height}}{\text{water colum depth}} \quad (4)$$

Duckweed cover% was estimated by eye, typically every 4 weeks.

2.11. Statistical analyses

Statistical analyses were carried out using Python and the R software environment (R-Core Team 2019). To estimate total GHG emissions for each ecological state, we summed CH_4 ebullition and diffusive water-atmosphere CH_4 and CO_2 fluxes as CO_2 equivalents, using a global warming potential (GWP) of 34 for CH_4 fluxes, corresponding to the radiative forcing over a 100-year time horizon (IPCC, 2013). Annual average CH_4 ebullition was calculated by summing CH_4 ebullition measured during each bubble collection period and dividing it by the number of days between start and end of bubble collection monitoring in that respective year (i.e. day of year [DOY] 1–336, 2–337 and 1–326 for algae, submerged plant and free-floating plant dominated systems, respectively). Measured diffusive fluxes of CH_4 and CO_2 were linearly interpolated between each measurement day (starting at DOY 5, 4, and 4, and ending at DOY 336, 332, and 325 for algae-, submerged plant- and free-floating plant-dominated systems, respectively) to obtain an estimate for each day. We then averaged these daily estimates to obtain an annual average daily flux estimate. The effect of experimental warming on annual daily GHG fluxes was analyzed using estimation statistics [Python package DABEST (Ho et al., 2019)].

To describe the temperature dependency of CH_4 ebullition for each system, we used a modified Arrhenius equation (Eq. (5)):

$$E_T = E_{20} * \theta_s^{(T-20)} \quad (5)$$

where E_T is the ebullition rate in mg CH_4 m^{-2} d^{-1}, at temperature T (°C), E_{20} is the ebullition rate in mg CH_4 m^{-2} d^{-1} at 20 °C, and θ_s is the overall system temperature coefficient (dimensionless) (Kadlec and Reddy, 2001; Veraart et al., 2011).

The modified Arrhenius expression was fitted on the data using the Levenberg-Marquardt nonlinear least-squares algorithm [function *nlsLM* from the R package minpack.lm (Elzhov et al., 2022)]. Despite its limitations at the lower and upper end of the temperature range, the modified Arrhenius expression is a useful and often-applied method of determining temperature dependencies of ecological and microbiological processes (Aben et al., 2017; Kadlec and Reddy, 2001; Veraart et al., 2011).

We used linear mixed-effects models (LMMs) to investigate the effect of different sets of predictors on water-atmosphere greenhouse gas fluxes. Here, limnotron and sampling date were included as crossed random effects on the intercept to account for repeated measurements in individual limnotrons (l) and across days (d), as below (Eq. (6)):

$$Y_{ld} = \beta_0 + L_{0l} + D_{0d} + \beta_1 X_{1d} + \beta_2 X_{2d} + \ldots + \beta_M X_M + \varepsilon_{ld} \quad (6)$$

Models were fitted with the *lmer* function from the R package lme4 (Bates et al., 2015), using maximum likelihood (ML). We used the *dredge* function (R package MuMIn (Bartoń, 2022)) to test models with all possible predictor combinations and ranked them by AICc-based model weight (Burnham and Anderson, 2002). To meet assumptions of linearity, homoscedasticity, and normality of residuals, fluxes were log- or square root transformed when necessary. To deal with mismatching predictor data due to different sampling dates, we linearly interpolated data using the *na.approx* function of the R package zoo (Zeileis and Grothendieck, 2005) for R, to obtain predictor data at dates of gas flux measurement. Values for ebullition represent average emissions of specific periods of bubble trap deployment (as explained earlier). To obtain predictor data that matched these ebullition measurements, we averaged the interpolated predictor data for each period of bubble trap deployment.

3. Results & discussion

3.1. CH_4 ebullition

CH_4 ebullition was the most important GHG emission pathway independent of the dominant plant type when considering both CO_2 and CH_4 emissions in CO_2-equivalents (Fig. 1a-c). Considering CH_4 alone (diffusion and ebullition), the share of ebullition ranged from 53% to over 99% (Table 1), which is similar to the range reported for shallow lakes and ponds measured globally (Zheng et al. (2022) and references therein). Annual average CH_4 ebullition rates were 9.3, 38.3 and 78.4 mg CH_4 m^{-2} d^{-1} under dominance of submerged plants, algae and free-floating plants, respectively (Fig. 1a), and are in the middle of the range measured in ponds in different climate zones around the world (Zheng et al., 2022). The effect size of experimental warming on annual CH_4 ebullition (as the absolute treatment difference) was much larger in the algae and free-floating plant-dominated systems than in those dominated by submerged plants (Fig. 1a). The relative effect of experimental warming was strongest in the submerged plant-dominated systems, where mean annual CH_4 ebullition was on average almost twice as high in the experimental warming treatment as in the control. The effect size in systems with submerged plants, however, has a confidence interval close to the zero-effect line, indicating that the effect of experimental warming on ebullition is not as evident as in the algae and free-floating plant-dominated systems (Fig. 2& Table S1). The absolute increase in CH_4 ebullition with increasing seasonal temperature was also much higher under dominance by either algae or free-floating plants than by submerged plants (Fig. 2& Fig. 3). CH_4 ebullition at 20 °C, as modelled by fitting an Arrhenius equation to our data, was highest for the free-floating plant-dominated state, followed by, respectively the algae-dominated and submerged plant-dominated state (Fig. 3). In all systems, CH_4 ebullition increased exponentially with warming which is in accordance with what has been found in—mostly unvegetated sites—in natural systems (Aben et al., 2017). Notably, however, ebullition started to increase at considerably higher temperatures in the submerged plant-dominated state than in the other states, resulting in a system temperature coefficient (θ_s) increasing from free-floating to algae to submerged plant-dominated states.

Although we took care to make sediment conditions largely equal (with the bulk sediment being harvested from the same source and ensuring near equal C:N ratio's) for the three functional plant types, small between-plant-treatment sediment variability may explain part of the difference in ebullition between the plant types. However, given that the increase in sediment mineralization with temperature is remarkably

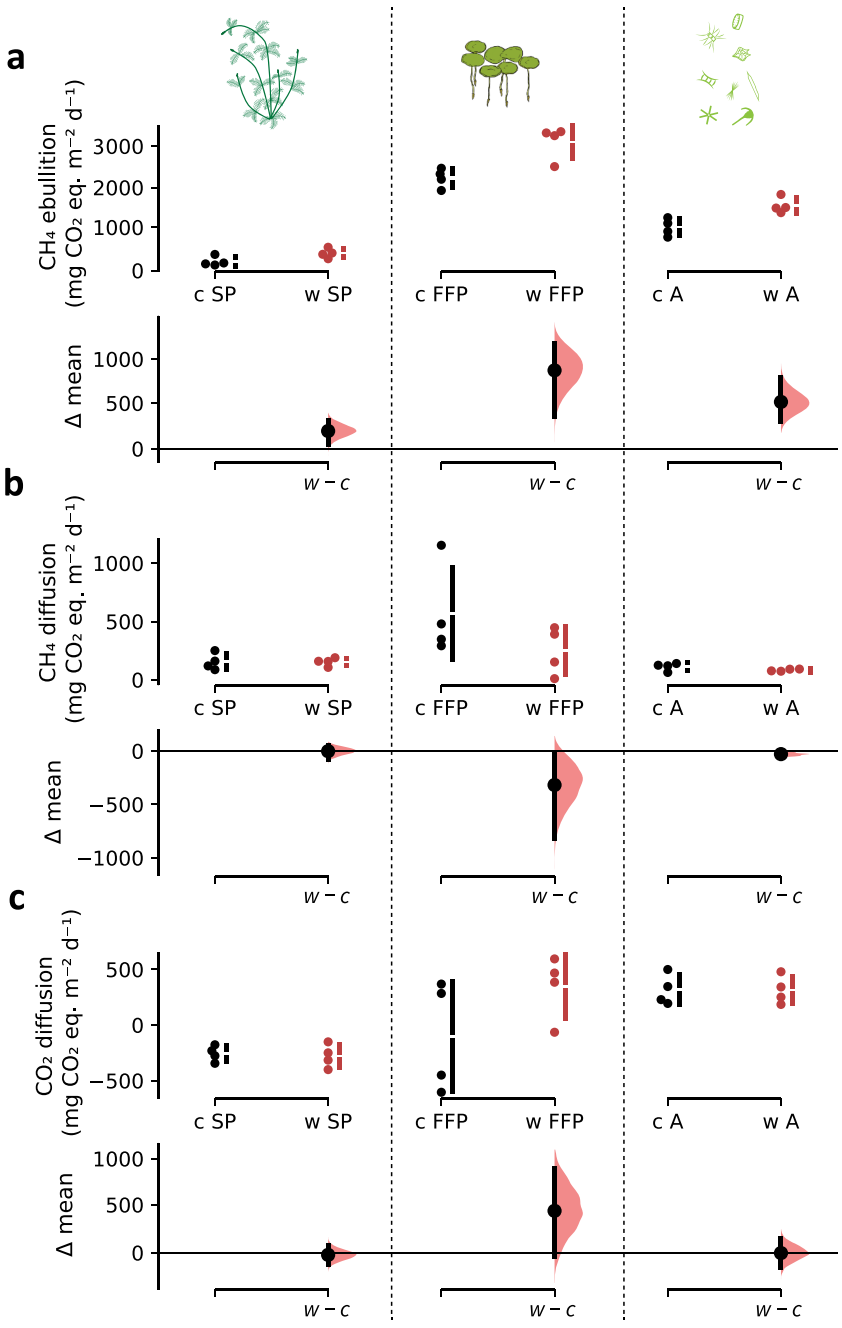

Fig. 1. The effect of 4 °C warming on annual mean (a) CH_4 ebullition and (b) water-atmosphere CH_4 diffusion, and (c) CO_2 diffusion, in systems dominated by different functional plant types. The top panel of each Cumming plot (Ho et al., 2019) shows the annual average flux for each mesocosm in the control (c) and +4 °C warming (w) treatment ($n = 4$) of the submerged plant (SP), free-floating plant (FFP) and algae (A) dominated state. To the right of each group are summary measurements (mean ± standard deviation), drawn as gapped lines. Each bottom panel shows the effect size as the mean treatment difference (w minus c) and its 95% confidence interval, displayed as a point estimate and vertical bar, respectively. The curve indicates the resampled distribution of the mean difference, given the observed data (5000 nonparametric bootstrap resamples). All values are expressed as CO_2 equivalents (CO_2 eq.). Positive CO_2 fluxes indicate that mesocosms were sources of CO_2 to the atmosphere, whilst negative fluxes denote they were sinks. For the free-floating plant-dominated state, diffusive and ebullitive CH_4 emissions were corrected for effects of plant-related bubble trapping (see Methods for details).

consistent for a wide range of sediments (Cardoso et al., 2014) and given the large plant effect on oxygen conditions and sedimentation rates in our setup (Table 1), we argue that a large share of the temperature effect on ebullition in our systems can be explained by the differential effects the dominant plant types have on carbon processes. Moreover, while sediment organic C was lower under algae dominance than under submerged plant dominance at the onset of the experiment (Table 1), CH_4 ebullition was much higher under algae dominance (Fig. 1). This further supports the notion that primary producer traits govern CH_4 ebullition.

The amount of biomass needed to establish an algae, submerged plant or free-floating plant dominated system varied (Table 1). Our findings, however, suggest that this did not explain the observed differences in CH_4 ebullition rates. For instance, while the algae-dominated systems had the lowest added biomass as well as the lowest final biomass and lowest carbon sedimentation rates (Table 1), they exhibited higher CH_4 ebullition rates than the submerged plant-dominated systems (Figs. 1, 2). In addition, while the carbon sedimentation rates in the free-floating plant-dominated systems and submerged plant-dominated systems were considerably higher than those in the algae-dominated systems (Table 1), the CH_4 ebullition rates between the free-floating plant-dominated and submerged plant-dominated systems deviated much more from each other than from the algae dominated systems (Figs. 1, 2). Also, when we normalize the average annual CH_4 ebullition for the amount of biomass (in grams of C) added to the systems we find that emissions for the submerged plant dominated systems are lowest and those for algae are highest (Fig. S5). These findings substantiate that primary producer traits strongly impact CH_4 production and consumption, and consequent CH_4 emissions, overruling effects of biomass. Lower ebullition rates in systems dominated by submerged plants may be explained by several mechanisms. First, radial oxygen loss (ROL) by the roots of submerged plants can oxidize the rhizosphere and thereby curtail CH_4 emission by stimulating CH_4 oxidation and inhibiting CH_4

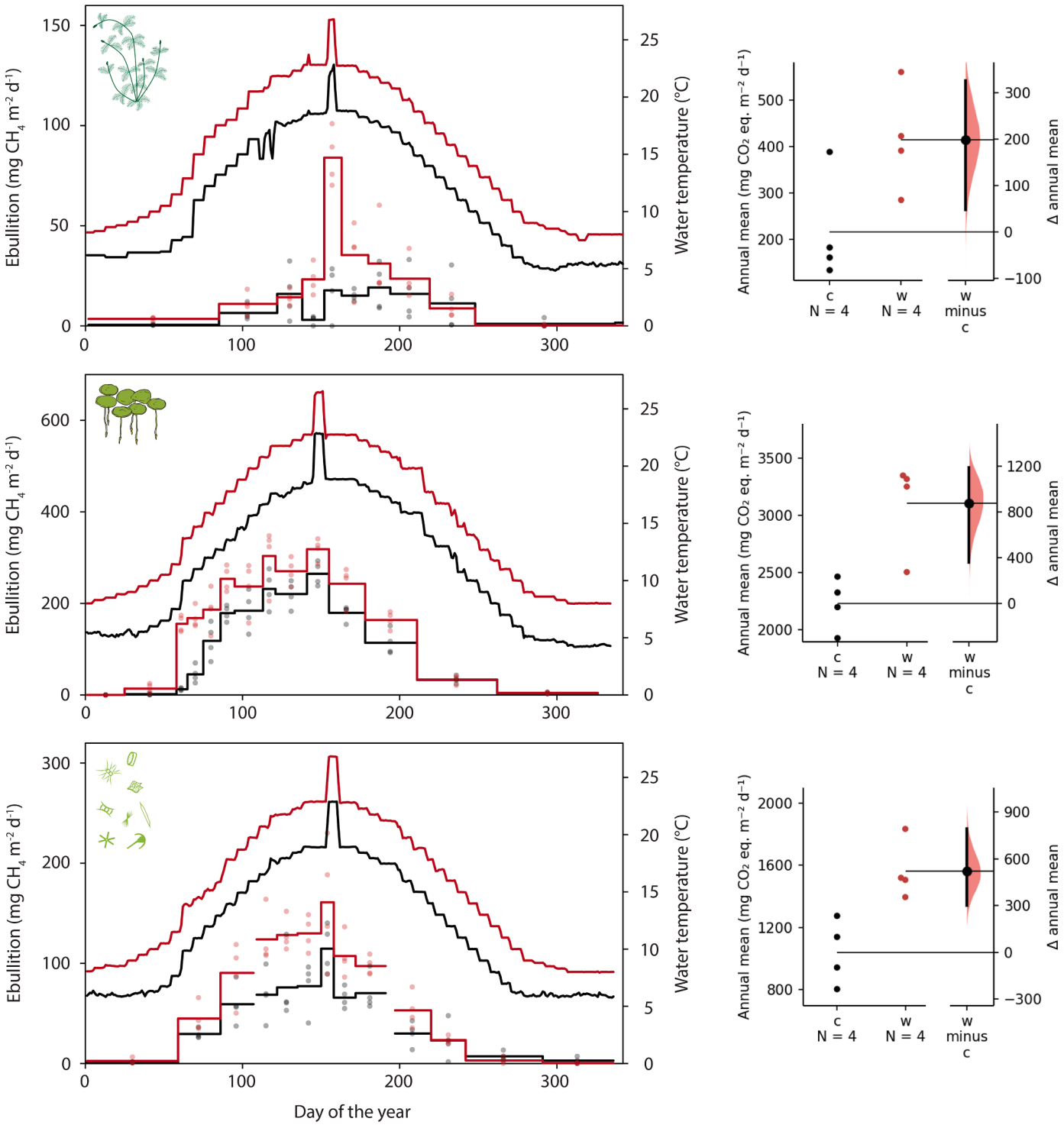

Fig. 2. CH_4 ebullition for the control and the warm (+4 °C) mesocosms under dominance of submerged plants, free-floating plants, and algae, respectively. Left: Red circles and lines (arithmetic mean) denote warm treatment, black ones denote control. Each dot represents the mean CH4 ebullition (as the average of two bubble trap measurements per mesocosm) for a given bubble trap deployment period of a given mesocosm. Upper lines denote water temperature for the control (black) and warm treatment (red). Peak temperatures represent a heat wave (+4 °C) that was applied to both treatments. Ebullition for the free-floating plant-dominated state represents raw data, not corrected for effects of plant-related bubble trapping (see Methods for details). Right: Gardner-Altman plots (Ho et al., 2019) showing annual average CH_4 ebullition for each mesocosm in the control (c) and +4 °C warming (w) treatment of each ecosystem state. The effect size (the mean treatment difference: w minus c) and its 95% confidence interval is displayed as a point estimate and vertical bar, respectively, on a separate but aligned axis. The curve indicates the resampled distribution of Δ, given the observed data (5000 nonparametric bootstrap resamples). The annual mean CH_4 ebullition for the free-floating plant--dominated state was corrected by 20% for plant-related bubble trapping (see Methods for details).

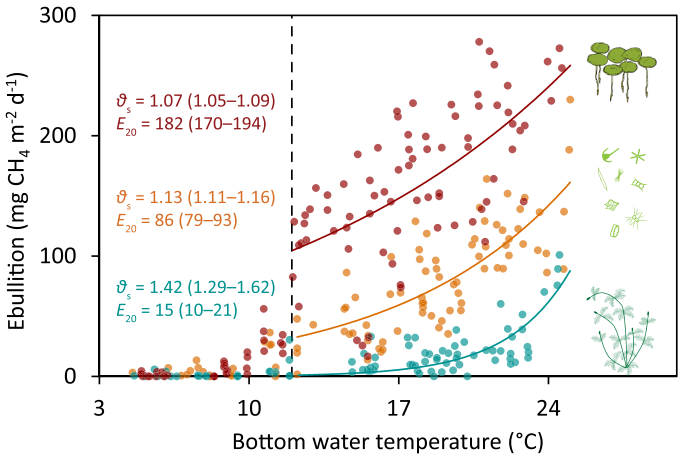

Fig. 3. Ebullitive CH_4 emissions expressed against water temperature. Brown, orange, and green dots represent mean CH4 ebullition (as the average of two bubble trap measurements per mesocosm) for each bubble trap deployment period of each mesocosm in states dominated by free-floating plants, algae, and submerged plants. The corresponding temperature represents the mean bottom water temperature during the bubble trap deployment. The dashed vertical line represents the onset of strongly increased ebullition. Regression lines represent a fitted modified Arrhenius expression; see Eq. (5) in Methods. E_{20} represents the modelled CH_4 ebullition at 20 °C and θ_s the overall system temperature coefficient. The Arrhenius equation was fitted on data starting from 12 °C as it overestimates ebullition below this temperature, particularly for systems dominated by free-floating plants. A threshold of 10–16 °C at which ebullition starts to increase exponentially with temperature has also been observed in other studies (Aben et al., 2017; DelSontro et al., 2010; Wang et al., 2021). Values in parentheses represent 95% confidence intervals. In the free-floating plant-dominated state, ebullition was adjusted downwards by 20% to account for the fraction of bubbles trapped under the dense plant mats (see Methods for details).

production (Calhoun and King, 1997; Dullo et al., 2017; Li et al., 2021). *Myriophyllum spicatum*, the species used in our experiment, has a high sediment-oxygenating potential (Mermillod-Blondin et al., 2008), with the intensity of its ROL mainly determined by oxygen concentration in the water column and redox condition and microbial oxygen demand in the sediment (Laskov et al., 2006). Indeed, our analyses show that both water column oxygen concentration and plant abundance (as PVI) were selected as important predictors that negatively affect ebullition and thus explain the emission patterns observed in our experiment (Table S2), which is in line with earlier observations (Davidson et al., 2018). Clearly, plant abundance does not necessarily reflect plant metabolic activity and ROL intensity. In our experiment a decline in PVI was preceded by peak ebullition rates (occurring at the highest temperatures in the warm treatment, see upper panel Fig. 2; see Velthuis et al. (2018) for PVI dynamics). This suggests that when plant conditions deteriorate (leading to a decline in PVI), so does the regulation effect of plants on CH_4 ebullition. We speculate that warming did not only have a direct effect on ebullition via enhanced CH_4 production, but that at the highest temperatures also a decrease in ROL occurred leading to less CH_4 oxidation. The presumed combined warming effects could also explain the high system temperature coefficient (θ_s) in the submerged plant treatment (Fig. 3). Second, transport of CH_4 through roots and shoots may limit ebullition by alleviating the build-up of gaseous CH_4 in the sediment (Dacey and Klug, 1979; Heilman and Carlton, 2001; Sanders et al., 2007). The occurrence of plant-mediated transport in our study was substantiated by the presence of CH_4 inside the plants. Plant-mediated CH_4 fluxes may partially end up in the water column where it can be oxidized (Li et al., 2021), or can be directly emitted to the atmosphere via the plants' inflorescences (Heilman and Carlton, 2001) (captured in our floating chamber measurements).

The highest CH_4 ebullition in our setup was observed in the state with free-floating plant dominance (Fig. 1a). This can likely be attributed to anaerobic mineralization of fresh organic matter sedimented at high rates (Table 1). Dense mats of free-floating plants have been shown to impede oxygen intrusion (de Tezanos Pinto and O'Farrell, 2014). Together with the high sediment oxygen demand associated with the high sedimentation rates, this may have led to oxygen-poor and even anoxic waters (Table 1). Water column anoxia is a common phenomenon during dominance by floating plants in natural systems (de Tezanos Pinto and O'Farrell, 2014). Such anoxic conditions promote CH_4 production and hamper aerobic CH_4 oxidation (Bastviken et al., 2009). This may lead to a decrease in the CH_4 concentration gradient from the sediment pore water to the overlaying water, resulting in a decrease in sediment-water CH_4 diffusion. The reduced diffusive release of CH_4 from the sediment in turn, may increase accumulation of free CH_4 gas and hence bubble release. This may explain why surface water oxygen concentration was shown to be an important predictor for ebullition when floating plants were dominant (Table S2). Anoxia also facilitates phosphorus release from sediments (Table 1) resulting in a positive feedback loop between duckweed cover, preferring high P concentrations, and P availability (Boedeltje et al., 2005; Kazanjian et al., 2018a).

3.2. *Diffusive CH_4 emissions*

Annual average CH_4 diffusion rates were 4.5, 2.9 and 12.0 mg CH_4 m^{-2} d^{-1} under dominance of submerged plants, algae and free-floating plants, respectively (Fig. 4). These fluxes are at the lower end of the range measured globally for small lakes (< 0.001 km^2) and ponds (on average around 36 mg CH_4 m^{-2} d^{-1} (Holgerson and Raymond, 2016; Zheng et al., 2022)). Diffusive CH_4 emissions correlated positively with seasonal changes in water temperature in both the 4 °C warming treatment and the ambient controls of all three states (Fig. 4). Despite this, the data show very little support for a positive effect of the 4 °C warming treatment in the three different states and, in fact, are most indicative for a negative effect of experimental warming in algae and free-floating plant-dominated states (Fig. 1b, Fig. 4 & Table S1). Diffusive CH_4 fluxes were particularly high when free-floating plants dominated (Fig. 1b), which is likely associated with the dissolution of CH_4 from bubbles trapped under the plant mats and the likely shallower oxygen penetration depth in the sediment due to water column hypoxia. Water column hypoxia below floating plants happens in a wide range of freshwater ecosystems ranging from ponds and ditches to tropical lakes (de Tezanos Pinto and O'Farrell, 2014; Rodríguez et al., 2012; Scheffer et al., 2003). Low oxygen concentrations in the water column results in a shallower zone for CH_4 oxidation at the sediment-water interface, the place where the majority of CH_4 oxidation is to be expected (Bastviken et al., 2009). In combination with the reduced water-atmosphere gas exchange (Kosten et al., 2016), this likely also explains the high CH_4 concentrations in the water column (Table 1). Dense free-floating plant coverage may reduce the water-atmosphere gas exchange by up to 90% (Kosten et al., 2016). Yet, despite this reduced gas exchange, the measured diffusive CH_4 fluxes strongly exceeded the calculated diffusive fluxes (based on CH_4 concentrations and air-water gas exchange velocities) during the warmer periods in our experiment (Fig. S6). This is very likely explained by diffusive release of CH_4 from bubbles trapped underneath the free-floating plant mats when ebullition is high (Fig. S7).

3.3. *Diffusive CO_2 fluxes*

In the submerged plant- and algae-dominated systems there was little evidence for an important effect of the experimental warming treatment on diffusive CO_2 fluxes. In systems with free-floating plants, the data best support a positive effect of experimental warming on CO_2 fluxes (Fig. 1c, Table S1 & Fig. 5). There were quite large differences in fluxes between the different ecosystem states. While the submerged plant-dominated systems showed net CO_2 uptake, the algae-dominated systems were net emitters of CO_2 (Fig. 1c) as a result of the relatively low

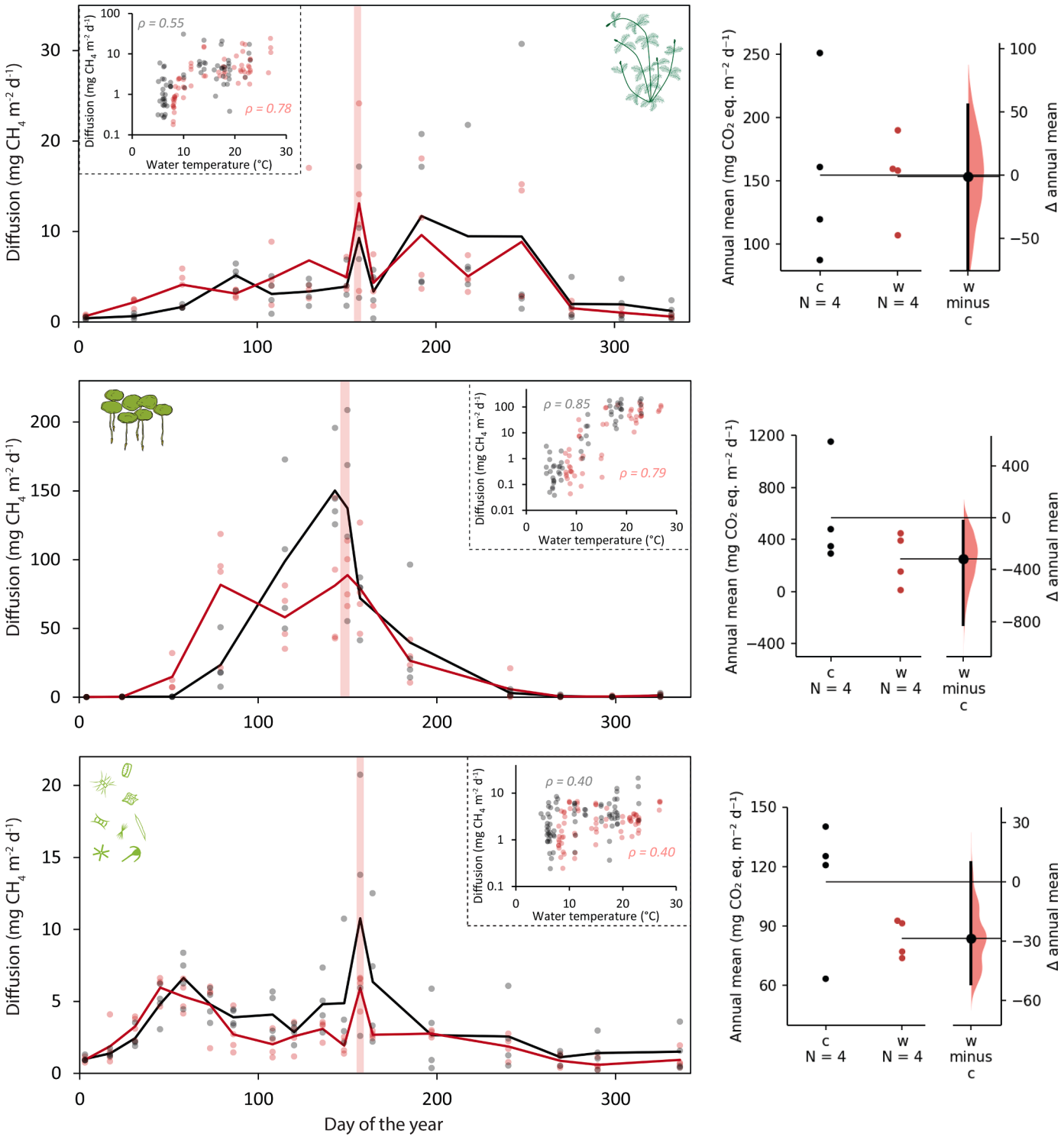

Fig. 4. Diffusive CH_4 emissions for the control and the warm (+4 °C) mesocosms under dominance of submerged plants, free-floating plants, and algae, respectively. Left: Red circles and lines (arithmetic mean) denote warm treatment, black ones denote control. Each dot represents the daily flux for a given mesocosm, calculated as a weighted mean (based on day- and nighttime length) of fluxes measured at the end of the light and dark period (see Methods for details). Red shading represents a heat wave (+4 °C) that was applied to both treatments. Top right scatter plots show the spearman correlation (ρ) between temperature and diffusive CH_4 emission in the control and warm treatment of each ecosystem state. Diffusive CH_4 emissions for the free-floating plant-dominated state represent raw data, not corrected for effects of plant related bubble trapping (see Methods for details). Right: Gardner-Altman plots (Ho et al., 2019) showing annual average diffusive CH_4 emission for each mesocosm in the control (c) and +4 °C warming (w) treatment of each ecosystem state. The effect size (the mean treatment difference: w minus c) and its 95% confidence interval is displayed as a point estimate and vertical bar, respectively, on a separate but aligned axis. The curve indicates the resampled distribution of Δ, given the observed data (5000 nonparametric bootstrap resamples). The annual mean diffusive CH_4 emission for the free-floating plant-dominated state was corrected for plant-related bubble trapping (see Methods for details).

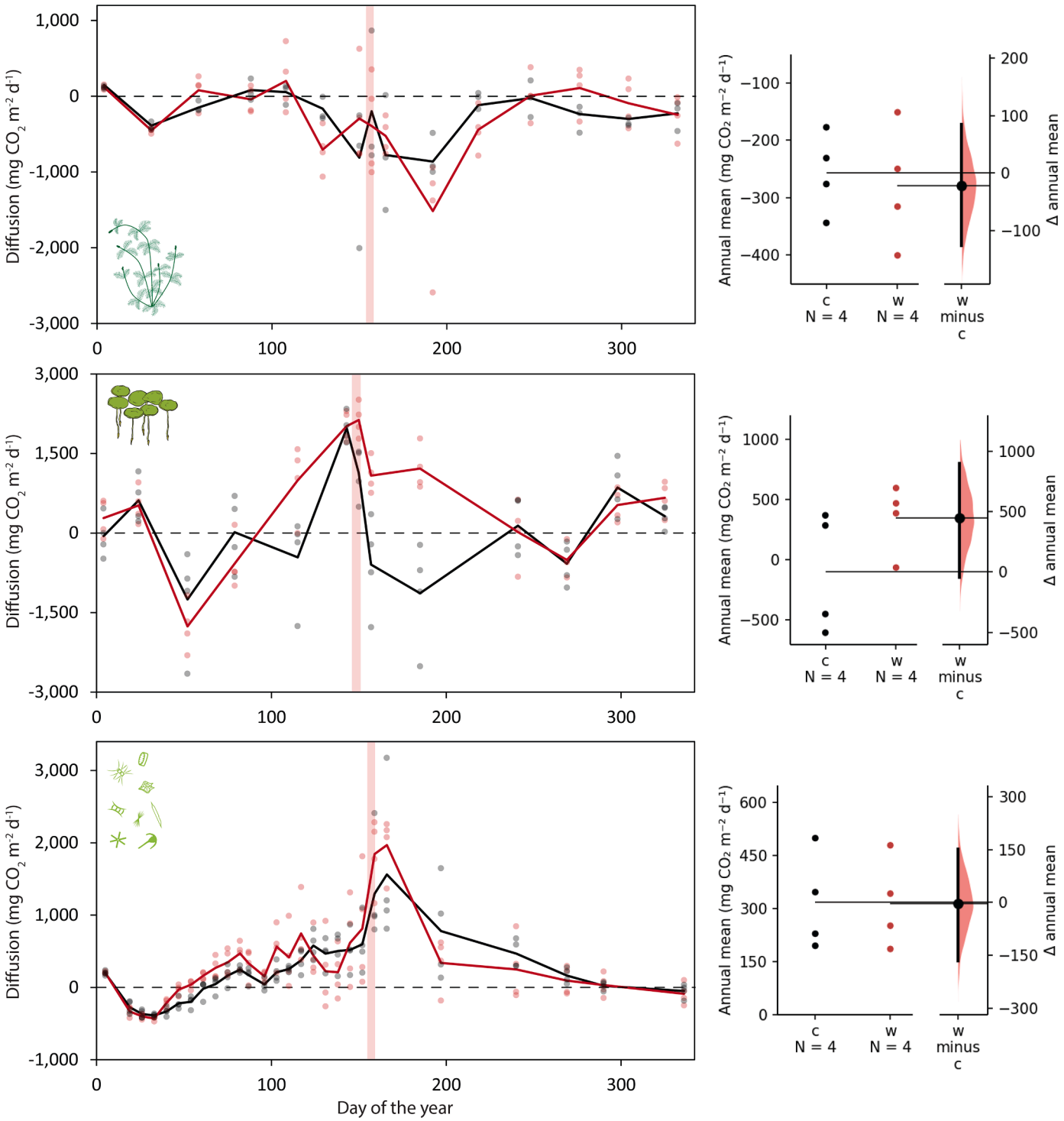

Fig. 5. Diffusive water-atmosphere CO_2 fluxes for the control and the warm (+4 °C) mesocosms under dominance of submerged plants, free-floating plants, and algae, respectively. Left: Red circles and lines (arithmetic mean) denote warm treatment, black ones denote control. Each dot represents the daily flux for a given mesocosm, calculated as a weighted mean (based on day- and nighttime length) of fluxes measured at the end of the light and dark period (see Methods for details). Red shading represents a heat wave (+4 °C) that was applied to both treatments. Values above and below the dashed line represent net CO_2 emission and uptake, respectively. Right: Gardner-Altman plots (Ho et al., 2019) showing the annual average diffusive CO_2 flux (mg CO_2 m^{-2} d^{-1}) for each mesocosm in the control (c) and +4 °C warming (w) treatment of each ecosystem state. The effect size (the mean treatment difference: w minus c) and its 95% confidence interval is displayed as a point estimate and vertical bar, respectively, on a separate but aligned axis. The curve indicates the resampled distribution of Δ, given the observed data (5000 nonparametric bootstrap resamples).

primary production (Kazanjian et al., 2018b). The latter was likely related to phosphorus limitation as demonstrated by surface water phosphate concentrations, which were very low throughout most of the year (Table 1) and resulted in higher seston N:P ratios (Velthuis et al., 2017). In contrast, rooted, submerged plants like the species in our experiment (*M. spicatum*) take up most of their N and P directly from the sediment via their root system (Barko et al., 1991). Indeed, annual average (± SD) N (as NH_4^+ + NO_3^-) and PO_4^{3-}-P concentrations in

sediment pore waters (3350 ± 1149 μg L^{-1} and 147 ± 36 μg L^{-1}, respectively) were an order of magnitude higher than in the water column (132 ± 19 μg L^{-1} and 25.0 ± 0.3 μg L^{-1}, respectively). Moreover, both N (3.4 ± 0.7%) and P (0.46 ± 0.17%) contents of dried plant shoots (mean ± s.d.) were far above values that are indicative of suboptimal growth, i.e. 0.75% and 0.07% for N and P, respectively (Gerloff, 1975). This indicates that primary production under dominance by submerged plants was likely not limited by N and P availability and can explain the observed net CO_2 uptake. The free-floating plant-dominated state shows large variation in CO_2 fluxes among replicates within both temperature treatments. This variation strongly exceeded that of the other two states (Figs. 1c, 5).

3.4. Combined GHG fluxes and water management implications

All in all, we show that the effect of warming on total GHG emissions from experimental ponds is greatest under dominance by free-floating plants and smallest when submerged plants dominate (Fig. 6), which can be mainly attributed to a differential temperature effect on methane ebullition. When comparing the different states, our findings suggest that the total GHG emissions decline going from free-floating plant, to algae, to submerged plant dominated state. These results can have major implications. As climate warming can both enhance CH_4 production rates (Aben et al., 2017; Davidson et al., 2018; Marotta et al., 2014) and favor free-floating plant or phytoplankton dominance over submerged plant dominance (Meerhoff et al., 2022), our results indicate that CH_4 emissions may be enhanced more than expected based on direct temperature effects alone. In our systems, the enhanced CH_4 emissions were not offset by an increase in CO_2 uptake. Hence, our findings suggest that the combined effect of warming and displacement of submerged plants by algae or free-floating plants exacerbates the increase in GHG emissions. This indicates a positive feed-back loop in which enhanced GHG emissions accelerate climate warming (Fig. 7). Notably, different plant traits (e.g. having roots that enable P-uptake from sediments and the ability to use HCO_3^- as C source) not only affect GHG emission and uptake, but also the resources available to the plants. Disentangling the direct and indirect plant effects on warming-induced changes in GHG emissions therefore remains complex.

The fact that GHG emissions were lowest in the submerged plant-dominated state, both under control and warmed conditions may have major implications for water management. Across the world, water managers target dominance by submerged plants as it generally coincides with higher water quality, clear water, higher biodiversity, and a broader range of ecosystem services (Janssen et al., 2021). This generally requires a combination of costly management strategies to maintain this ecosystem state (e.g. external and internal nutrient load reduction, fish community manipulation and/or harvesting free-floating plants) (Hilt et al., 2018; Smolders et al., 2006). The benefits of mitigating GHG emissions by the restoration of submerged vegetation (Fig. 7) can provide additional leverage and even outweigh their costs (Downing et al., 2021), as the measures may eventually result in a situation beneficial from an ecological, societal, and climate perspective.

4. Conclusions

- Shifts from submerged plant to algae or free-floating plant dominance may increase the magnitude and temperature sensitivity of GHG emissions from shallow aquatic ecosystems. This may trigger a positive feedback loop as climate change is expected to enhance shifts to algae or free-floating plant dominance.
- CH_4 ebullition was the most important GHG emission pathway, both in terms of emission magnitude and its sensitivity to experimental warming. Hence, we stress the need for accurate quantification of CH_4 ebullition at high spatiotemporal scales as well as technological

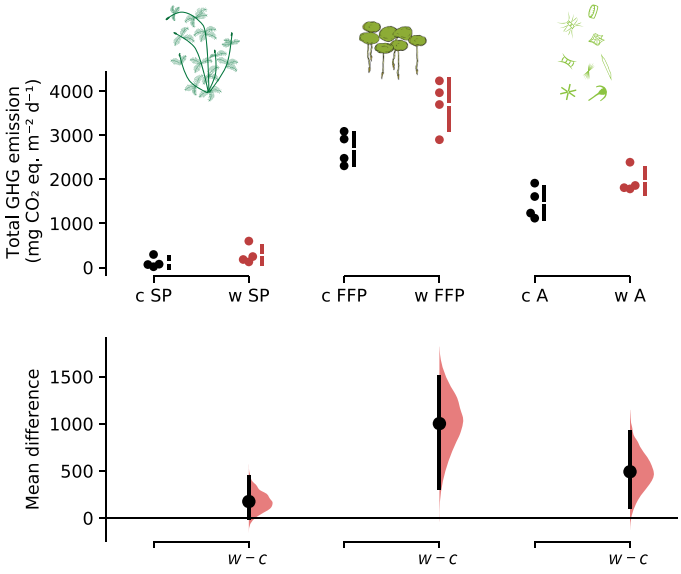

Fig. 6. Effect of climate warming and dominance of different types of plants on annual greenhouse gas (GHG) emissions. The top panel of the Cumming plot (Ho et al., 2019) shows annual average total GHG emission for each mesocosm in the control (c) and +4 °C warming (w) treatment of the submerged plant (SP), free-floating plant (FFP) and algae (A) dominated state. To the right of each group are summary measurements (mean ± standard deviation), drawn as gapped lines. The bottom panel shows the effect size as the mean treatment difference (w minus c) and its 95% confidence interval, displayed as a point estimate and vertical bar, respectively. The curve indicates the resampled distribution of the mean difference, given the observed data (5000 nonparametric bootstrap resamples). Total GHG emissions are expressed as CO_2 equivalents (CO_2 eq.).

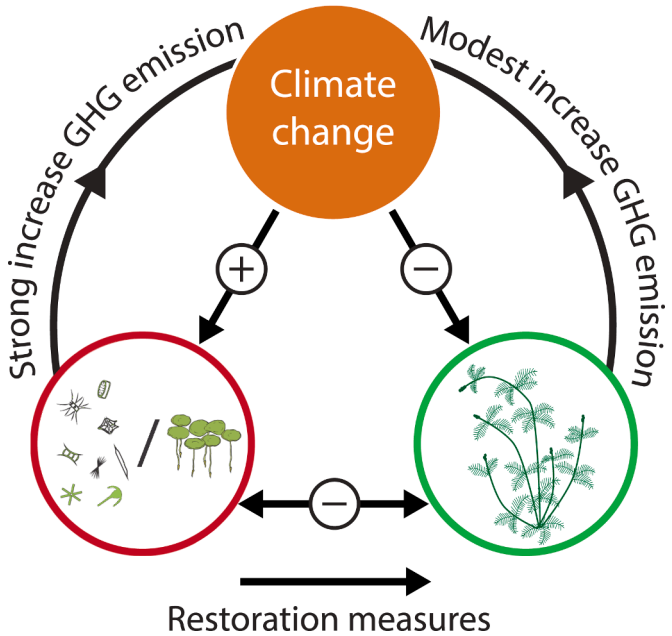

Fig. 7. Interactions between climate change, regime shifts, and GHG emissions. Climate change favours dominance by algae and floating plants at the expense of submerged plants. Restoration measures establishing dominance by submerged plants in shallow aquatic ecosystems can moderate the positive feedback loop between climate change and aquatic GHG emissions. Plus (+) and minus (-) symbols denote stimulating and inhibiting effects, respectively. Each dominant plant type self-stabilizes their state through a variety of feedback mechanisms, thereby inhibiting a shift to dominance of other functional plant types.

advances that ease the quantification of CH_4 bubble fluxes to the atmosphere in floating plant beds.
- Restoration of submerged vegetation may limit increases in GHG emissions due to climate change.

CRediT authorship contribution statement

Ralf C.H. Aben: Data curation, Investigation, Formal analysis, Visualization, Writing – original draft. **Mandy Velthuis:** Data curation, Investigation, Writing – review & editing. **Garabet Kazanjian:** Formal analysis, Visualization, Writing – review & editing. **Thijs Frenken:** Writing – review & editing. **Edwin T.H.M. Peeters:** Writing – review & editing. **Dedmer B. Van de Waal:** Writing – review & editing. **Sabine Hilt:** Writing – review & editing. **Lisette N. de Senerpont Domis:** Writing – review & editing, Writing – review & editing. **Leon P.M. Lamers:** Writing – review & editing. **Sarian Kosten:** Conceptualization, Supervision, Writing – original draft.

Declaration of Competing Interest

The authors declare that they have no known competing financial interests or personal relationships that could have appeared to influence the work reported in this paper.

Data availability

The data that support the findings of this study are archived in the DANS EASY repository: https://doi.org/10.17026/dans-zqj-dyrc.

Acknowledgments

We thank F. Rust de Carvalho, F. Xue and N. Helmsing for their assistance during the mesocosm experiment. The work of M.V. was funded by the Gieskes-Strijbis Foundation and NWO-Veni grant 202.053. G.K.'s funding was provided by the Leibniz Association - project Landscales. S.K. was supported by Nederlandse Organisatie voor Wetenschappelijk Onderzoek (NWO) [Veni grant No. 86312012]. Submerged plant and algae symbols in article figures were designed by Tracey Saxby, IAN Image Library (ian.umces.edu/imagelibrary/).

Supplementary materials

Supplementary material associated with this article can be found, in the online version, at doi:10.1016/j.watres.2022.119251.

References

Aben, R.C.H., Barros, N., van Donk, E., Frenken, T., Hilt, S., Kazanjian, G., Lamers, L.P. M., Peeters, E.T.H.M., Roelofs, J.G.M., de Senerpont Domis, L.N., Stephan, S., Velthuis, M., Van de Waal, D.B., Wik, M., Thornton, B.F., Wilkinson, J., DelSontro, T., Kosten, S., 2017. Cross continental increase in methane ebullition under climate change. Nat. Commun. 8 (1), 1682.
Allen, A.P., Gillooly, J.F., Brown, J.H., 2005. Linking the global carbon cycle to individual metabolism. Funct. Ecol. 19 (2), 202–213.
Arts, G.H.P., van de Hoek, T.H., Schot, J.A., Sinkeldam, J.A., Verdonschot, P.F.M., 2001. Biotic responses to eutrophication and recovery in outdoor experimental ditches. In: Internationale Vereinigung für Theoretische und Angewandte Limnologie: Verhandlungen, 27, pp. 3492–3496.
Bade, D.L., Cole, J.J., 2006. Impact of chemically enhanced diffusion on dissolved inorganic carbon stable isotopes in a fertilized lake. J. Geophys. Res. 111 (C01014).
Barko, J.W., Gunnison, D., Carpenter, S.R., 1991. Sediment interactions with submersed macrophyte growth and community dynamics. Aquat. Bot. 41 (1), 41–65.
Bartoń, Kamil, 2022. MuMIn: Multi-Model Inference. R package version 1.46.0. The Comprehensive R Archive Network (CRAN), Vienna, Austria.
Bastviken, David, 2009. Methane. In: Likens, Gene E. (Ed.), Encyclopedia of Inland Waters. Academic Press, pp. 783–805. ISBN: 9780123706263.
Bates, D., Maechler, M., Bolker, B., Walker, S., 2015. Fitting linear mixed-effects models using {lme4}. J. Stat. Softw. 67 (1), 1–48.
Bodmer, P., Vroom, R., Stepina, T., del Giorgio, P.A. and Kosten, S. 2021. Methane fluxes of vegetated areas in natural freshwater ecosystems: assessments and global significance.
Boedeltje, G., Smolders, A.J., Lamers, L.P., Roelofs, J.G., 2005. Interactions between sediment propagule banks and sediment nutrient fluxes explain floating plant dominance in stagnant shallow waters. Arch. Hydrobiol. 162 (3), 349–362.
Burnham, K.P., Anderson, D.R., 2002. Model Selection and Multimodel Inference: a Practical Information-Theoretic Approach. Springer, New York.
Calhoun, A., King, G.M., 1997. Regulation of root-associated methanotrophy by oxygen availability in the rhizosphere of two aquatic macrophytes. Appl. Environ. Microbiol. 63 (8), 3051–3058.
Canfield Jr, D.E., Shireman, J.V., Colle, D.E., Haller, W.T., Watkins Ii, C.E., Maceina, M.J, 1984. Prediction of chlorophyll a concentrations in Florida lakes: importance of aquatic macrophytes. Can. J. Fish. Aquat. Sci. 41 (3), 497–501.
Cardoso, S.J., Enrich-Prast, A., Pace, M.L., Roland, F., 2014. Do models of organic carbon mineralization extrapolate to warmer tropical sediments? Limnol. Oceanogr. 59 (1), 48–54.
Carpenter, S.R., Lodge, D.M., 1986. Effects of submersed macrophytes on ecosystem processes. Aquat. Bot. 26, 341–370.
Cole, J.J., Bade, D.L., Bastviken, D., Pace, M.L., Van de Bogert, M., 2010. Multiple approaches to estimating air-water gas exchange in small lakes. Limnol. Oceanogr. 8 (6), 285–293.
Curran, J. 2013 Bolstad2: Bolstad functions. R package version 1.0-28.
Dacey, J.W.H., Klug, M.J., 1979. Methane efflux from lake sediments through water lilies. Science 203 (4386), 1253–1255.
Davidson, T.A., Audet, J., Jeppesen, E., Landkildehus, F., Lauridsen, T.L., Søndergaard, M., Syväranta, J., 2018. Synergy between nutrients and warming enhances methane ebullition from experimental lakes. Nat. Clim. Change 8 (2), 156–160.
Davidson, T.A., Audet, J., Svenning, J.C., Lauridsen, T.L., Søndergaard, M., Landkildehus, F., Larsen, S.E., Jeppesen, E., 2015. Eutrophication effects on greenhouse gas fluxes from shallow-lake mesocosms override those of climate warming. Glob. Change Biol. 21 (12), 4449–4463.
de Tezanos Pinto, P., O'Farrell, I, 2014. Regime shifts between free-floating plants and phytoplankton: a review. Hydrobiologia 740 (1), 13–24.
DelSontro, T., Boutet, L., St-Pierre, A., del Giorgio, P.A., Prairie, Y.T., 2016. Methane ebullition and diffusion from northern ponds and lakes regulated by the interaction between temperature and system productivity. Limnol. Oceanogr. 61 (S1), S62–S77.
DelSontro, T., McGinnis, D.F., Sobek, S., Ostrovsky, I., Wehrli, B., 2010. Extreme methane emissions from a Swiss hydropower reservoir: contribution from bubbling sediments. Environ. Sci. Technol. 44 (7), 2419–2425.
Dossena, M., Yvon-Durocher, G., Grey, J., Montoya, J.M., Perkins, D.M., Trimmer, M., Woodward, G., 2012. Warming alters community size structure and ecosystem functioning. In: Proceedings of the Royal Society B: Biological Sciences, 279, pp. 3011–3019.
Downing, J.A., Polasky, S., Olmstead, S.M., Newbold, S.C., 2021. Protecting local water quality has global benefits. Nat. Commun. 12 (1), 2709.
Dullo, B.W., Grootjans, A.P., Roelofs, J.G.M., Senbeta, A.F., Fritz, C., Lamers, L.P.M., 2017. Radial oxygen loss by the cushion plant Eriocaulon schimperi prevents methane emissions from an East-African mountain mire. Plant Biol. 19 (5), 736–741.
Fuchs, A., Lyautey, E., Montuelle, B., Casper, P., 2016. Effects of increasing temperatures on methane concentrations and methanogenesis during experimental incubation of sediments from oligotrophic and mesotrophic lakes. J. Geophys. Res. 121 (5), 1394–1406.
Gerloff, G.C, 1975. Nutritional Ecology of Nuisance Aquatic Plants. National Environmental Research Center, Office of Research and Development, US Environmental Protection Agency.
Gilbert, P.J., Taylor, S., Cooke, D.A., Deary, M.E., Jeffries, M.J., 2021. Quantifying organic carbon storage in temperate pond sediments. J. Environ. Manag. 280, 111698.
Grasshoff, K., Johannsen, H., 1972. A new sensitive and direct method for the automatic determination of ammonia in sea water. ICES J. Mar. Sci. 34 (3), 516–521.
Heilman, M.A., Carlton, R.G., 2001. Ebullitive release of lacunar gases from floral spikes of Potamogeton angustifolius and Potamogeton amplifolius: effects on plant aeration and sediment CH4 flux. Aquat. Bot. 71 (1), 19–33.
Henriksen, A., 1965. An automatic method for determining low-level concentrations of phosphates in fresh and saline waters. Analyst 90 (1066), 29–34.
Hilt, S., Alirangues Nuñez, M.M., Bakker, E.S., Blindow, I., Davidson, T.A., Gillefalk, M., Hansson, L.-A., Janse, J.H., Janssen, A.B.G., Jeppesen, E., Kabus, T., Kelly, A., Köhler, J., Lauridsen, T.L., Mooij, W.M., Noordhuis, R., Phillips, G., Rücker, J., Schuster, H.-H., Søndergaard, M., Teurlincx, S., van de Weyer, K., van Donk, E., Waterstraat, A., Willby, N., Sayer, C.D., 2018. Response of submerged macrophyte communities to external and internal restoration measures in north temperate shallow lakes. Front. Plant Sci. 9.
Hilt, S., Brothers, S., Jeppesen, E., Veraart, A.J., Kosten, S., 2017. Translating regime shifts in shallow lakes into changes in ecosystem functions and services. Bioscience 67 (10), 928–936.
Ho, J., Tumkaya, T., Aryal, S., Choi, H., Claridge-Chang, A., 2019. Moving beyond P values: data analysis with estimation graphics. Nat. Methods 16 (7), 565–566.
Holgerson, M.A., Raymond, P.A., 2016. Large contribution to inland water CO_2 and CH_4 emissions from very small ponds. Nat. Geosci. 9 (3), 222–226.
Hood, J.M., Benstead, J.P., Cross, W.F., Huryn, A.D., Johnson, P.W., Gíslason, G.M., Junker, J.R., Nelson, D., Ólafsson, J.S., Tran, C., 2018. Increased resource use efficiency amplifies positive response of aquatic primary production to experimental warming. Glob. Change Biol. 24 (3), 1069–1084.

Hussner, A., 2012. Alien aquatic plant species in European countries. Weed Res. 52 (4), 297–306.
Elzhov, T.V., Mullen, K.M., Spiess, A. and Bolker, B. 2022. minpack. lm: R Interface to the Levenberg-Marquardt Nonlinear Least-Squares Algorithm Found in MINPACK. R Packag. version 1.2-2.
IPCC 2013 Climate Change 2013: the physical science basis. Contribution of working group I to the fifth assessment report of the intergovernmental panel on climate change. Stocker, T.F., D. Qin, G.-K. Plattner, M. Tignor, S.K. Allen, J. Boschung et al. (ed), p. 1535.
Istvánovics,, V., 2009. Eutrophication of Lakes and Reservoirs. Encyclopedia of Inland Waters. Academic Press.
Janssen, A.B.G., Hilt, S., Kosten, S., de Klein, J.J.M., Paerl, H.W., Van de Waal, D.B., 2021. Shifting states, shifting services: linking regime shifts to changes in ecosystem services of shallow lakes. Freshw. Biol. 66 (1), 1–12.
Kadlec, R.H., Reddy, K., 2001. Temperature effects in treatment wetlands. Water Environ. Res. 73 (5), 543–557.
Kamphake, L.J., Hannah, S.A., Cohen, J.M., 1967. Automated analysis for nitrate by hydrazine reduction. Water Res. 1 (3), 205–216.
Kazanjian, G., Flury, S., Attermeyer, K., Kalettka, T., Kleeberg, A., Premke, K., Köhler, J., Hilt, S., 2018a. Primary production in nutrient-rich kettle holes and consequences for nutrient and carbon cycling. Hydrobiologia 806 (1), 77–93.
Kazanjian, G., Velthuis, M., Aben, R., Stephan, S., Peeters, E.T.H.M., Frenken, T., Touwen, J., Xue, F., Kosten, S., Van de Waal, D.B., de Senerpont Domis, L.N., van Donk, E., Hilt, S., 2018b. Impacts of warming on top-down and bottom-up controls of periphyton production. Sci. Rep. 8 (1), 9901.
Kosten, S., Piñeiro, M., de Goede, E., de Klein, J., Lamers, L.P.M., Ettwig, K., 2016. Fate of methane in aquatic systems dominated by free-floating plants. Water Res. 104, 200–207.
Kraemer, B.M., Mehner, T., Adrian, R., 2017. Reconciling the opposing effects of warming on phytoplankton biomass in 188 large lakes. Sci. Rep. 7 (1), 10762.
Laskov, C., Horn, O., Hupfer, M., 2006. Environmental factors regulating the radial oxygen loss from roots of Myriophyllum spicatum and Potamogeton crispus. Aquat. Bot. 84 (4), 333–340.
Li, Y., Shang, J., Zhang, C., Zhang, W., Niu, L., Wang, L., Zhang, H., 2021. The role of freshwater eutrophication in greenhouse gas emissions: a review. Sci. Total Environ. 768, 144582.
Lofton, D.D., Whalen, S.C., Hershey, A.E., 2014. Effect of temperature on methane dynamics and evaluation of methane oxidation kinetics in shallow Arctic Alaskan lakes. Hydrobiologia 721 (1), 209–222.
Marotta, H., Pinho, L., Gudasz, C., Bastviken, D., Tranvik, L.J., Enrich-Prast, A., 2014. Greenhouse gas production in low-latitude lake sediments responds strongly to warming. Nat. Clim. Change 4 (6), 467–470.
Meerhoff, M., Audet, J., Davidson, T.A., De Meester, L., Hilt, S., Kosten, S., Liu, Z., Mazzeo, N., Paerl, H., Scheffer, M., 2022. Feedback between climate change and eutrophication: revisiting the allied attack concept and how to strike back, Inland. Inland Waters 12 (2), 187–204.
Mermillod-Blondin, F., Lemoine, D., Boisson, J.-.C., Malet, E., Montuelle, B., 2008. Relative influences of submersed macrophytes and bioturbating fauna on biogeochemical processes and microbial activities in freshwater sediments. Freshw. Biol. 53 (10), 1969–1982.
Millero, F.J., Graham, T.B., Huang, F., Bustos-Serrano, H., Pierrot, D., 2006. Dissociation constants of carbonic acid in seawater as a function of salinity and temperature. Mar. Chem. 100 (1), 80–94.
Mooij, W.M., Janse, J.H., De Senerpont Domis, L.N., Hülsmann, S., Ibelings, B.W., 2007. Predicting the effect of climate change on temperate shallow lakes with the ecosystem model PCLake. Hydrobiologia 584 (1), 443–454.
Murphy, J., Riley, J.P., 1962. A modified single solution method for the determination of phosphate in natural waters. Anal. Chim. Acta 27, 31–36.
Netten, J.J.C., Arts, G.H.P., Gylstra, R., van Nes, E.H., Scheffer, M., Roijackers, R.M.M., 2010. Effect of temperature and nutrients on the competition between free-fl oating *Salvinia natans* and submerged *Elodea nuttallii* in mesocosms. Fundam. Appl. Limnol. 177 (2), 125–132.
Netten, J.J.C., Van Zuidam, J., Kosten, S., Peeters, E.T.H.M., 2011. Differential response to climatic variation of free-floating and submerged macrophytes in ditches. Freshw. Biol. 56 (9), 1761–1768.
Nieuwenhuize, J., Maas, Y.E.M., Middelburg, J.J., 1994. Rapid analysis of organic carbon and nitrogen in particulate materials. Mar. Chem. 45 (3), 217–224.
Nixdorf, B., Arndt, H., 1993. Seasonal changes in the plankton dynamics of a eutrophic lake including the microbial web. Int. Rev. Ges. Hydrobiol. Hydrogr. 78 (3), 403–410.
Peeters, E.T.H.M., van Zuidam, J.P., van Zuidam, B.G., Van Nes, E.H., Kosten, S., Heuts, P.G.M., Roijackers, R.M.M., Netten, J.J.C., Scheffer, M., 2013. Changing weather conditions and floating plants in temperate drainage ditches. J. Appl. Ecol. 50 (3), 585–593.
Rodríguez, P., Pizarro, H., Vera, M.S., 2012. Size fractionated phytoplankton production in two humic shallow lakes with contrasting coverage of free floating plants. Hydrobiologia 691 (1), 285–298.
Sander, R., 2015. Compilation of Henry's law constants (version 4.0) for water as solvent. Atmos. Chem. Phys. 15 (8), 4399–4981.
Sanders, I.A., Heppell, C.M., Cotton, J.A., Wharton, G., Hildrew, A.G., Flowers, E.J., Trimmer, M., 2007. Emission of methane from chalk streams has potential implications for agricultural practices. Freshw. Biol. 52 (6), 1176–1186.
Saunois, M., Jackson, R.B., Bousquet, P., Poulter, B., Canadell, J.G., 2016. The growing role of methane in anthropogenic climate change. Environ. Res. Lett. 11 (12), 120207.
Scheffer, Marten, 1998. Ecology of Shallow Lakes, 1st. Springer, Dordrecht, pp. 1–357.
Scheffer, M., Carpenter, S.R., 2003. Catastrophic regime shifts in ecosystems: linking theory to observation. Trends Ecol. Evol. 18 (12), 648–656.
Scheffer, M., Szabó, S., Gragnani, A., van Nes, E.H., Rinaldi, S., Kautsky, N., Norberg, J., Roijackers, R.M.M., Franken, R.J.M., 2003. Floating plant dominance as a stable state. Proc. Natl. Acad. Sci. U. S. A. 100 (7), 4040–4045.
Scheffer, M., van Nes, E.H., 2007. Shallow lakes theory revisited: various alternative regimes driven by climate, nutrients, depth and lake size. Hydrobiologia 584 (1), 455–466.
Shelley, F., Abdullahi, F., Grey, J., Trimmer, M., 2015. Microbial methane cycling in the bed of a chalk river: oxidation has the potential to match methanogenesis enhanced by warming. Freshw. Biol. 60 (1), 150–160.
Smolders, A., Lamers, L., Lucassen, E., Van der Velde, G., Roelofs, J., 2006. Internal eutrophication: how it works and what to do about it—a review. Chem. Ecol. 22 (2), 93–111.
Stumm, W., Morgan, J.J., 1996. Chemical Equilibria and Rates in Natural Waters. Aquatic Chemistry, 3rd. John Wiley & Sons, pp. 1–1040.
Tóth, V.R., Herodek, S., 2011. Seasonal shift of dominance in a submerged rooted macrophyte community of Lake Balaton. Ann. Limnol. Int. J. Limnol. 47 (2), 141–150.
Tribe, L., Briens, C., Margaritis, A., 1995. Determination of the volumetric mass transfer coefficient (kLa) using the dynamic "gas out–gas in" method: analysis of errors caused by dissolved oxygen probes. Biotechnol. Bioeng. 46 (4), 388–392.
Velthuis, M., de Senerpont Domis, L.N., Frenken, T., Stephan, S., Kazanjian, G., Aben, R., Hilt, S., Kosten, S., van Donk, E., Van de Waal, D.B., 2017. Warming advances top-down control and reduces producer biomass in a freshwater plankton community. Ecosphere 8 (1), e01651.
Velthuis, M., Kosten, S., Aben, R., Kazanjian, G., Hilt, S., Peeters Edwin, T.H., Van, M., Donk, E., Bakker, E.S, 2018. Warming enhances sedimentation and decomposition of organic carbon in shallow macrophyte-dominated systems with zero net effect on carbon burial. Glob. Change Biol. 24 (11), 5231–5242.
Veraart, A.J., De Klein, J.J., Scheffer, M., 2011. Warming can boost denitrification disproportionately due to altered oxygen dynamics. PLoS One 6 (3), e18508.
Verschoor, A.M., Takken, J., Massieux, B., Vijverberg, J., 2003. The Limnotrons: a facility for experimental community and food web research. Hydrobiologia 491 (1–3), 357–377.
Vollenweider, R., Kerekes, J., 1980. Background and Summary Results of the OECD Cooperative Program on Eutrophication. US Environmental Protection Agency Washington, pp. 5–81.
Wang, G., Xia, X., Liu, S., Zhang, L., Zhang, S., Wang, J., Xi, N., Zhang, Q., 2021. Intense methane ebullition from urban inland waters and its significant contribution to greenhouse gas emissions. Water Res. 189, 116654.
Wanninkhof, R., 2014. Relationship between wind speed and gas exchange over the ocean revisited. Limnol. Oceanogr. 12 (6), 351–362.
Wik, M., Thornton, B.F., Bastviken, D., Uhlbäck, J., Crill, P.M., 2016. Biased sampling of methane release from northern lakes: a problem for extrapolation. Geophys. Res. Lett. 43 (3), 1256–1262.
Yvon-Durocher, G., Allen, A.P., Bastviken, D., Conrad, R., Gudasz, C., St-Pierre, A., Thanh-Duc, N., Del Giorgio, P.A., 2014. Methane fluxes show consistent temperature dependence across microbial to ecosystem scales. Nature 507 (7493), 488–491.
Yvon-Durocher, G., Hulatt, C.J., Woodward, G., Trimmer, M., 2017. Long-term warming amplifies shifts in the carbon cycle of experimental ponds. Nat. Clim. Change 7 (3), 209–213.
Yvon-Durocher, G., Jones, J.I., Trimmer, M., Woodward, G., Montoya, J.M., 2010. Warming alters the metabolic balance of ecosystems. In: Philosophical Transactions of the Royal Society B: Biological Sciences, 365, pp. 2117–2126.
Zeileis, A., Grothendieck, G., 2005. Zoo: S3 Infrastructure for regular and irregular time series. J. Stat. Softw. 14 (6), 1–27.
Zheng, Y., Wu, S., Xiao, S., Yu, K., Fang, X., Xia, L., Wang, J., Liu, S., Freeman, C., Zou, J., 2022. Global methane and nitrous oxide emissions from inland waters and estuaries. Glob. Change Biol. 28 (15), 4713–4725.
Zhu, Y., Purdy, K.J., Eyice, Ö., Shen, L., Harpenslager, S.F., Yvon-Durocher, G., Dumbrell, A.J., Trimmer, M., 2020. Disproportionate increase in freshwater methane emissions induced by experimental warming. Nat. Clim. Change 10 (7), 685–690.